Journal of Power Sources 196 (2011) 3443–3447

Contents lists available at ScienceDirect

Journal of Power Sources

journal homepage: www.elsevier.com/locate/jpowsour

Short communication

Measurement of three-dimensional microstructure in a $LiCoO_2$ positive electrode

James R. Wilson [a], J. Scott Cronin [a], Scott A. Barnett [a,*], Stephen J. Harris [b]

[a] Department of Materials Science and Engineering, Northwestern University, 2220 Campus Drive, Evanston, IL 60208, USA
[b] General Motors R&D Center, M/C 480-102-000, Warren, MI 48090, USA

ARTICLE INFO

Article history:
Received 23 March 2010
Accepted 20 April 2010
Available online 28 April 2010

Keywords:
Lithium-ion batteries
Three-dimensional (3D) microstructure
Focused ion beam (FIB) tomography
$LiCoO_2$
Electrodes

ABSTRACT

In this work we elucidate the 3D microstructure of the $LiCoO_2$ phase in a fresh commercial Li-ion battery positive electrode using a focused ion beam-scanning electron microscope. The particles have a highly irregular shape that includes significant internal cracking. These cracks provide a higher surface area for Li charge transfer, and they provide alternate pathways for Li transport within particles. In addition, the cracks would substantially alter the stress distributions within particles during Li-insertion and make the particles more susceptible to fracture. The particles were typically made up of multiple grains whose boundaries may also affect intraparticle Li-ion transport and fracture strength. While the particles do contact each other, the cross-sectional area of contact is quite small, emphasizing the importance of binder and conductive carbon for providing structural integrity to the electrode.

1. Introduction

Numerous properties of Li-ion battery electrodes depend on their microstructure. The size distribution, shape, internal structure, and packing arrangement of the constituent electrode particles are expected to impact various electrode properties, including conductivity (ionic, electronic, and thermal) charge capacity (volumetric and gravimetric), charging rate, internal stress distribution during lithiation, fracture strength, and degradation rate. Nonetheless, there have been only limited efforts to accurately measure electrode microstructure. Yoshizawa [1] used three-dimensional transmission electron tomography to observe the internal structure and connectivity of carbon nanospheres that have been used as an electrode material. Kostecki and McLarnon [2] showed that mechanical damage from the swelling and shrinking of electrode materials on each cycle may depend on particle location within the electrode. They also found [3] that swelling and shrinking of electrode material during cycling could cause agglomeration of the conductive carbon leading to loss of electrical connectivity. Zhang et al. [4] used focused ion beam (FIB) milling combined with EDS to demonstrate the presence of cracks in graphite particles that allowed electrolyte to enter, as evidenced by the presence of SEI on the walls of the cracks. Thorat et al. [5] made a direct measurement of the tortuosity of separators and electrodes.

The limited availability of microstructural data has had significant effects on battery models. For example, macro-homogeneous models generally assume that electrodes and active particles are homogeneous, isotropic, and flawless [6,7]. There have been a number of modeling efforts aimed at including more detailed microstructural information, particularly for relating microstructural changes and cell failure. White et al. [8] showed that cell degradation rates can be modeled as a reduction in porosity, caused perhaps by a growing SEI layer. Several groups [9–11] have studied the impact that Li intercalation can have on internal particle stresses that could lead to fracture. Sastry et al. [12–14] modeled packing and interparticle frictional forces among active particles assuming, for example, a random arrangement of solid ellipsoids. They predicted that calendering forces can be sufficient to cause particle fracture. All of these models would benefit from direct microstructural data.

Recently, focused ion beam-scanning electron microscopy (FIB-SEM) has been used to obtain three-dimensional microstructural information from solid oxide fuel cells [15–18]. The 3D measurements have the advantage of providing data that is more quantitative than two-dimensional electron microscope images. Furthermore, the 3D images are the only way to obtain information on features such as percolation, particle connectivity, and phase tortuosity, which play key roles in determining electrode performance.

Here we provide the first quantitative three-dimensional microstructural data for a positive electrode in a Li-ion battery. The $LiCoO_2$ electrode was taken from a commercial laptop battery. $LiCoO_2$ is the most commonly used positive electrode material for commercial cells. The results provide new perspectives on some of the assumptions that are commonly made in modeling Li-ion batteries.

* Corresponding author. Tel.: +1 847 491 2447; fax: +1 847 491 7820.
E-mail address: s-barnett@northwestern.edu (S.A. Barnett).

0378-7753/$ – see front matter © 2010 Elsevier B.V. All rights reserved.
doi:10.1016/j.jpowsour.2010.04.066

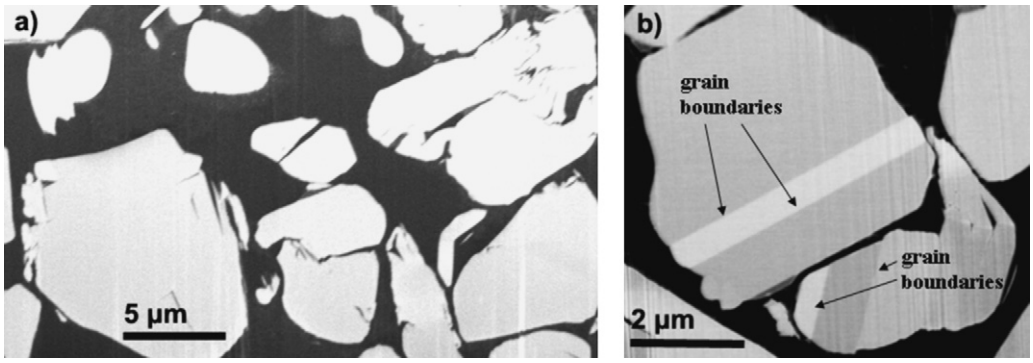

Fig. 1. (a) An image of the $LiCoO_2$ particles taken using the TLD detector on the FEI Helios instrument. (b) A standard secondary electron detector image from the Zeiss NVision instrument of $LiCoO_2$ particles showing clear contrast between grains within particles.

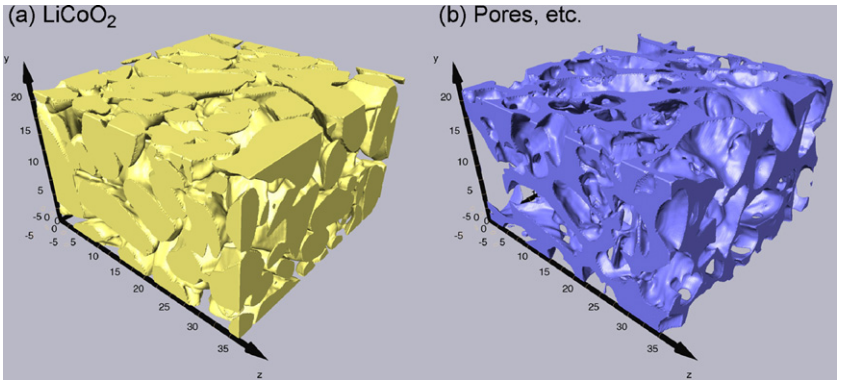

Fig. 2. (a and b) Three-dimensional images of the reconstructed volume showing the $LiCoO_2$ particle network on the left, and the inverse image on the right, with the porosity, carbon, and all other materials shown in blue (scale bars are in μm).

2. Materials and methods

A new Tianjin Lishen LR1865AH 18650 laptop battery was fully discharged and opened in a glove box, and a piece was cut from the positive $LiCoO_2$ electrode. The electrolyte solvent was allowed to evaporate. The electrode was not washed in order to minimize the chances that dissolution of remaining solvent, binder, SEI or other components might alter the electrode microstructure. The selected piece of electrode was vacuum infiltrated with a commercial epoxy resin (Buehler EpoThin) in order to fill the open porosity. The sample was then mounted on a standard SEM stub and sputter-coated with gold to avoid charging.

The sample was serial-sectioned in a FIB-SEM, yielding a series of two-dimensional images that were aligned, segmented, and stacked together to obtain 3D images [16,19]. A relatively large-volume low-resolution 3D image reconstruction was collected using an FEI Helios FIB-SEM in order to obtain good statistics on average electrode microstructural parameters. The images were collected using the Thru-the-Lens (TLD) detector in secondary electron mode. The image volume was 28,100 μm^3 and the resolution was 50 nm in the X and Y directions (SEM image resolution) and 200 nm in the Z direction (FIB slice direction/thickness). The relationship between the volume analyzed and the errors in microstructural calculations was analyzed in a similar manner to that published previously [20]. It was determined that the volume percentage and surface area density calculations had an error of less than 5%. Higher-resolution images were collected using a Zeiss Nvision FIB-SEM in order to achieve more detailed structural information on individual $LiCoO_2$ particles. In this case, the Everhart-Thornley secondary electron detector was used. Here, the image volume was 1700 μm^3 and the resolution was ~20 nm in the X and Y directions and ~60 nm in the Z direction.

For EBSD analysis, the sample was cross-sectioned and polished using the FEI Helios FIB-SEM. After initial milling using a 30 kV ion beam, the sample was tilted an additional ~8° and etched with a 5 kV ion beam in order to remove the amorphous surface damage that resulted from the higher energy milling. EBSD data was collected using an FEI Quanta ESEM instrument.

3. Results

Fig. 1(a) shows a representative 2D section from the large-volume FIB-SEM data set. In each 2D SEM image collected, the $LiCoO_2$ showed clearly as a light colored phase, while the rest of the material, comprised of epoxy filled porosity, binder, conductive carbon, and any non-volatile electrolyte residue, appeared black. The SEI is not detected here because its thickness is only ~10 nm. There were also clear contrast variations within particles, under some imaging conditions, as seen in Fig. 1(b). We associate this contrast with different crystallographic orientations. That is,

Table 1
$LiCoO_2$ individual particle structural data.

	Particle 1	Particle 2	Particle 3
Volume (μm^2)	38.0	38.1	58.0
Surface area (μm^2)	72.5	72.7	133.7
% Greater surface area than a sphere	32.7	32.7	84.6
% Surface area due to internal cracks	17.7	5.3	15.4
Vol% that is closer to a crack	23.2	7.0	13.7
% Reduction in total diffusion length due to cracks	16.0	2.6	9.0
Average diffusion length (μm)	0.271	0.439	0.313

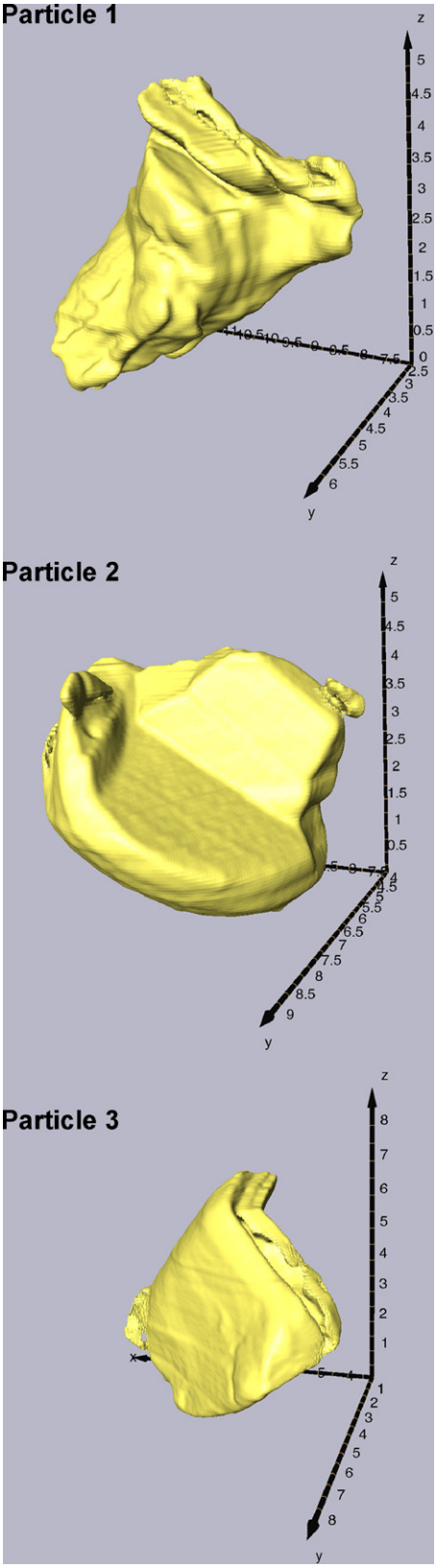

Fig. 3. 3D images of the reconstructions of three individual $LiCoO_2$ particles.

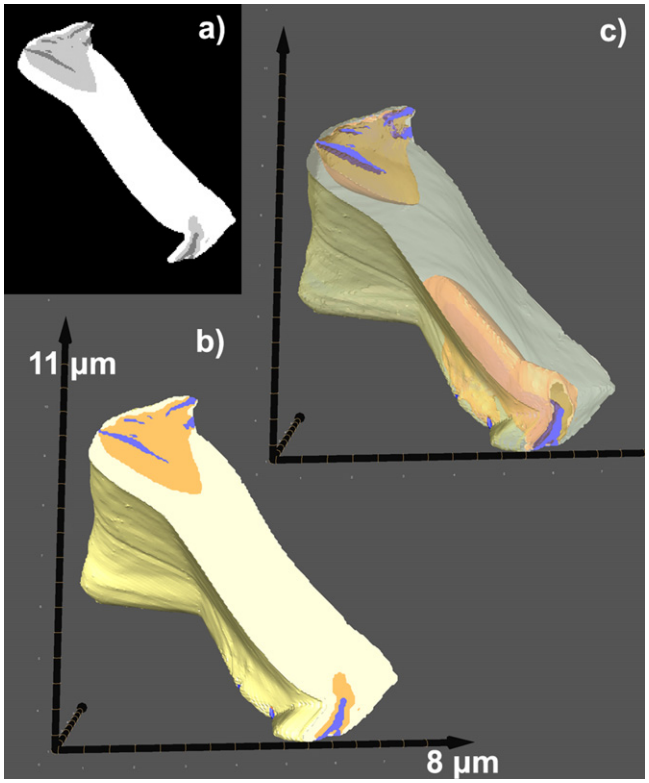

Fig. 4. (a) A 2D cross-sectional image of a single section showing the carbon-based materials (epoxy, conductive carbon, *etc.*) as black; the internal volume of $LiCoO_2$ that is closer to an internal crack, compared to the outside surface, colored as light gray; the rest of the $LiCoO_2$ particle in white; and the internal cracks are colored dark gray. (b) A 3D image of ~half the particle, cross-sectioned at the same plane as shown in (a). The internal cracks are in blue, the volume of $LiCoO_2$ closer to cracks are in orange, and the rest of the particle is yellow. (c) The same image as in part (b) but with the yellow and orange phases shown transparent in order to highlight the volume of the internal cracks throughout the particle. (For interpretation of the references to color in this figure legend, the reader is referred to the web version of the article.)

many of the particles were polycrystalline with numerous grain boundaries.

A three-dimensional image of each of the reconstructed phases is shown in Fig. 2. The $LiCoO_2$ phase constitutes 68.4% of the volume. The average specific surface area of the $LiCoO_2$ particles is 0.60 μm^{-1}, which corresponds to an average particle diameter of 6.8 μm if the particles are assumed to be spherical. The actual non-spherical shape of the particles leads to a higher surface area, with the result that this estimate yields a smaller average particle dimension than that observed in the images. The 3D images also allow a direct assessment of the connectivity of the phases [19]. Analysis of the $LiCoO_2$ connectivity shows that all of the particles are connected throughout the volume analyzed, although the contact areas were generally very small. Note that analysis of 2D images can yield the wrong result in this case because they often miss the small area of contact. This is readily seen in Fig. 1, where the $LiCoO_2$ particles do not appear to touch other particles. This emphasizes the importance of structural verification using 3D data. The black phase comprises 32.6% of the volume. If we estimate, very roughly, that the conductive carbon, electrolyte solvent, and binder take up half of the black phase, then the estimated electrode porosity is rather low, ~15%, but we note that this value is close to that found for the negative (graphite) electrode in this battery using X-ray tomography [21]. It will be interesting to see whether calculations that have been used to model particle architecture in electrodes assuming spheres and ellipsoids [12] can replicate the packing architecture

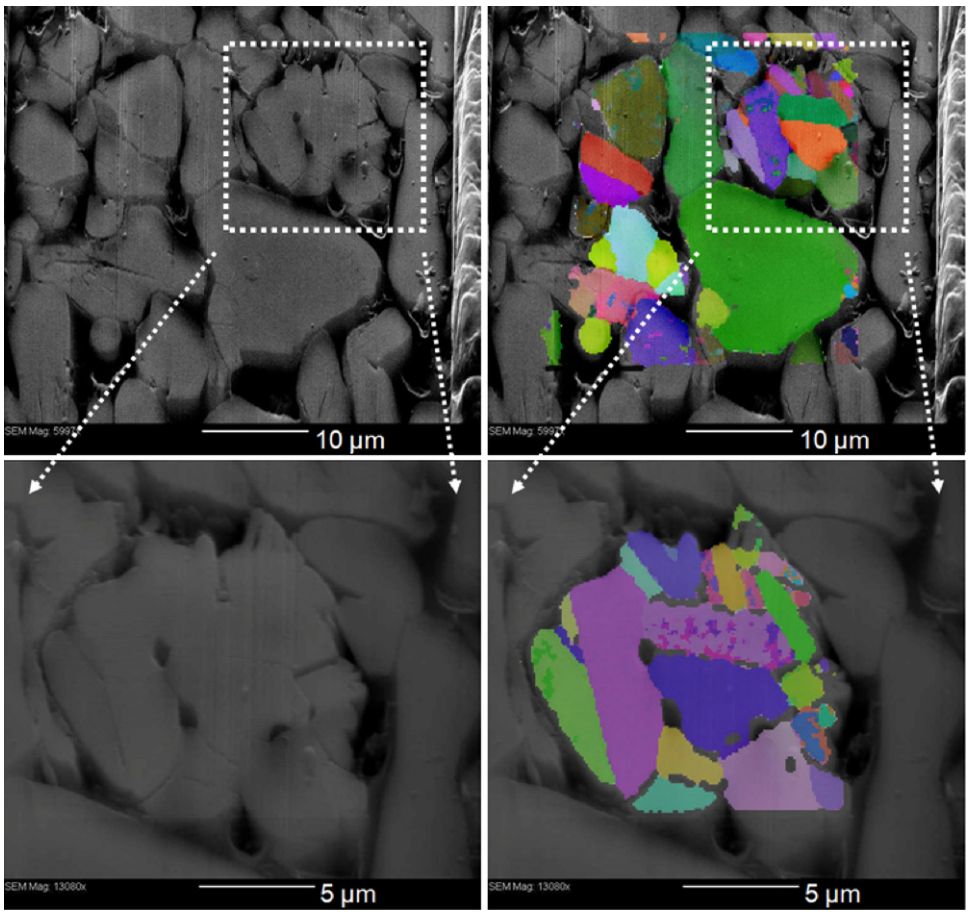

Fig. 5. SEM micrographs and EBSD colored overlays of a FIB-polished $LiCoO_2$ positive electrode cross-section. The bottom images are a zoomed-in multi-grained particle from the original low-resolution images shown on top.

and porosity that we observe, or whether more accurate representations of these very complex-shaped particles is required.

Fig. 3 shows 3D images of three individual $LiCoO_2$ particles. Videos showing these particles in three dimensions are available at www.LithiumBatteryResearch.com. The full complexity of these particles may not be apparent from just the 2D images of Fig. 1. A summary of the structural data for each of the three particles is provided in Table 1, showing the volumes and total surface areas. These particles have complex surface morphologies that add to the total surface area. The measured surface areas were substantially higher – 33%, 33%, and 85%, respectively – than spheres with the same volumes.

Within each of the particles, internal cracks are clearly visible in Figs. 1(a) and 4(a), even though the battery is nominally unused, beyond the forming step. (We take the presence of conformal surfaces facing each other to be evidence of a crack within a single particle, as opposed to two separate particles that happen to be near each other.) The existence of so many cracks in a nominally unused electrode is consistent with the prediction of Sastry et al. that the calendering process could lead to particle fracture even in the absence of any electrochemical cycling [22], although the cracks could equally well have been created during the forming process. The percentage of surface area contributed by internal cracks is 17.7%, 5.3%, and 15.4% for the three particles, respectively, in Table 1. All visible cracks appeared to be completely filled by the epoxy, indicating that the cracks were fully connected to the outsides of the particles. The presence of well-connected cracks indicates that the electrolyte had access to the particle interiors. Thus, additional electrolyte/$LiCoO_2$ surface area is available for charge transfer. In addition, the presence of electrolyte-filled cracks reduces the average distance Li must diffuse to fully lithiate/delithiate the particle, potentially improving the charge and discharge kinetics. On the other hand, there is more area for interfacial degradation reactions such as those discussed by Aurbach [23,24].

In order to help quantify these latter points, an analysis was conducted to determine the shortest diffusion distances from each point within a particle to different surfaces. Fig. 4(a) shows an example of a cross-sectional image from one of the particles. Regions where the shortest path is to an external surface are shown in white, whereas areas where the shortest path is to an internal crack are shown in grey. The average diffusion distance was calculated both including the internal cracks and neglecting them; the results showed that the presence of cracks decreased the average Li diffusion distance by 16.0%, 2.6%, and 9.0% for the three particles described in Table 1. Fig. 4(b) and (c) shows the full 3D image of particle #3, with the internal cracks in blue, the volume of $LiCoO_2$ that is closer to the cracks than the external boundary in orange, and the rest of the particle in transparent yellow. If there is further fracturing of these particles as the cell ages, diffusion distances would decrease by larger factors.

A similar argument can be made that grain boundaries within the particles can enhance Li transport; measurements on other oxides have shown that Li-grain boundary diffusion is substantially faster than bulk diffusion [25]. Fig. 5 shows EBSD data on a cross-section of the $LiCoO_2$ positive electrode. The low-resolution images in the top section of Fig. 5 show that there is a mix of single-grained and multiple-grained particles of $LiCoO_2$. A relationship between cracks and grain boundaries is shown in the lower section

of Fig. 5, from which it is clear that cracks are present along the grain boundaries. Finally, on a speculative note, the cracks may impact the particle mechanical properties. That is, the cracks will affect stresses that can develop from volume contraction and expansion during battery charge and discharge [26]. Internal cracks may promote particle fracture, an important degradation mechanism [27–30], by substantially reducing particle strength [26].

4. Discussion

Transport of Li from the exterior to the interior of particles is generally analyzed with the "shrinking core" model, which assumes that particles are internally solid, isotropic, and flawless. Under these conditions, intraparticle transport can be described as radial bulk diffusion [7]. It is recognized that this model is not appropriate for anisotropic-diffusion materials such as $LiFePO_4$ [7,31–33]. The present results indicate that it may be necessary to develop models that take into account the highly non-spherical, anisotropic, and defect-laden nature of primary or secondary electrode particles. In particular, the higher surface area and smaller bulk diffusion lengths in the actual non-spherical particles should substantially affect lithiation/delithiation kinetics.

One can also speculate as to the role of the cracks on degradation. In principle, if additional cracks are formed during cycling, the above effects that enhance charge/discharge kinetics could actually be magnified. However, it is also possible that the presence of cracks can exacerbate degradation mechanisms. For example, the presence of cracks in electrode particles after cycling has been taken to be a sign that fracture is an important degradation mechanism [28,29,34]. This is certainly likely for negative electrode materials such as Si and Sn, which can decrepitate under cycling, and perhaps for graphite where additional SEI formed on fracture surfaces could deplete the battery of Li [4]. It is less obvious what sort of role fracture plays for positive electrode particles. Fracture and degradation have been associated in some cases [28,34], and the creation of new surface area may lead to enhanced dissolution of the positive electrode in some cases [35].

5. Conclusions

In this work a three-dimensional serial-sectioning FIB-SEM technique was used to reconstruct the microstructure of a $LiCoO_2$ positive electrode from a fresh commercial Li-ion battery. Averaged parameters for the $LiCoO_2$ were obtained, including phase volume fraction and surface area. The other electrode phases, *i.e.*, carbon and binder, were not observed, but it may be possible to do so in the future if sufficient contrast can be achieved. The oxide particles were found to have small-area interparticle contacts. They had highly irregular shapes and significant internal cracking, leading to higher surface areas and reduced average Li diffusion lengths compared to spherical particles as normally assumed in electrode models. Grain boundaries were also observed, and these boundaries may also provide short-circuit transport paths for Li within the particles. The FIB-SEM method may become useful for quantitatively studying electrode microstructural changes resulting from charge-discharge cycling, and thereby help to understand degradation mechanisms.

Acknowledgments

The authors gratefully acknowledge the financial support of the National Science Foundation Ceramics program through grant DMR-0907639 (Northwestern Univ.) and the Initiative for Sustainability and Energy at Northwestern (ISEN). The FIB–SEM (Zeiss) was accomplished at the Electron Microscopy Center for Materials Research at Argonne National Laboratory, a U.S. Department of Energy Office of Science Laboratory operated under Contract No. DE-AC02-06CH11357 by UChicago Argonne, LLC. The FIB-SEM (FEI) was performed in the EPIC facility of NUANCE Center at Northwestern University. NUANCE Center is supported by NSF-NSEC, NSF-MRSEC, Keck Foundation, the State of Illinois, and Northwestern University.

References

[1] N. Yoshizawa, O. Tanaike, H. Hatori, K. Yoshikawa, A. Kondo, T. Abe, Carbon 44 (2006) 2558.
[2] R. Kostecki, F. McLarnon, J. Power Sources 119 (2003) 550.
[3] R. Kostecki, F. McLarnon, Electrochem. Solid-State Lett. 7 (2004) A38.
[4] H. Zhang, F. Li, C. Liu, J. Tan, H. Cheng, J. Phys. Chem. B 109 (2005) 22205.
[5] I. Thorat, D. Stephenson, N. Zacharias, K. Zaghib, J. Harb, D. Wheeler, J. Power Sources 188 (2009) 592.
[6] M. Doyle, T. Fuller, J. Newman, J. Electrochem. Soc. 140 (1993) 1526.
[7] V. Srinivasan, J. Newman, J. Electrochem. Soc. 151 (2004) A1517.
[8] G. Sikha, B. Popov, R. White, J. Electrochem. Soc. 151 (2004) A1104.
[9] J. Christensen, J. Newman, J. Electrochem. Soc. 153 (2006) A1019.
[10] Y. Cheng, M. Verbrugge, J. Appl. Phys. 104 (2008) 83521.
[11] X. Zhang, W. Shyy, A.M. Sastry, J. Electrochem. Soc. 154 (2007) A910.
[12] Y. Yi, C. Wang, A.M. Sastry, J. Electrochem. Soc. 151 (2004) A1292.
[13] Y.B. Yi, C.-W. Wang, A.M. Sastry, J. Eng. Mater. Technol. 128 (2006) 73.
[14] K. Striebel, A. Sierra, J. Shim, C.-W. Wang, A.M. Sastry, J. Power Sources 134 (2004) 241.
[15] J.R. Wilson, A.T. Duong, M. Gameiro, H.Y. Chen, K. Thornton, D.R. Mumm, S.A. Barnett, Electrochem. Commun. 11 (2009) 1052–1056.
[16] J.R. Wilson, W. Kobsiriphat, R. Mendoza, H.Y. Chen, J.M. Hiller, D.J. Miller, K. Thornton, P.W. Voorhees, S.B. Adler, S.A. Barnett, Nat. Mater. 5 (2006) 541–544.
[17] D. Gostovic, J. Smith, D. Kundinger, K. Jones, E. Wachsman, Electrochem. Solid-State Lett. 10 (2007) B214.
[18] J.R. Wilson, J.S. Cronin, A.T. Duong, S. Rukes, H.-Y. Chen, K. Thornton, D. Mumm, S.A. Barnett, J. Power Sources 195 (2010) 1829–1840.
[19] J.R. Wilson, M. Gameiro, K. Mischaikow, W. Kalies, P.W. Voorhees, S.A. Barnett, Microsc. Microanal. 15 (2009) 71–77.
[20] J.R. Wilson, W. Kobsiriphat, R. Mendoza, H.-Y. Chen, T. Hines, J.M. Hiller, D.J. Miller, K. Thornton, P.W. Voorhees, S.B. Adler, D. Mumm, S.A. Barnett, in: K. Eguchi, Singhal, S.C., Yokokawa, H., Mizusaki, J. (Ed.) Solid Oxide Fuel Cells 10 (SOFC-X), The Electrochemical Society, Nara, Japan, 2007, pp. 1879–1887.
[21] P.R. Shearing, L.E. Howard, P.S. Jørgensen, N.P. Brandon, S.J. Harris, Electrochem. Commun. 12 (2010) 374.
[22] C.-W. Wang, Y.B. Yi, A.M. Sastry, J. Shim, K. Striebel, J. Electrochem. Soc. 151 (2004) 1489.
[23] D. Aurbach, J. Power Sources 89 (2000) 206.
[24] D. Arubach, B. Markovsky, G. Salitra, E. Markevich, Y. Talyossef, J. Power Sources 165 (2007) 491.
[25] T. Okumura, T. Fukutsuka, Y. Uchimoto, N. Sakai, K. Yamaji, H. Yokokawa, J. Power Sources 189 (2009) 643–645.
[26] S.J. Harris, R. Deshpande, Y. Qi, I. Dutta, Y.-T. Cheng, J. Mater. Res., accepted for publication.
[27] T. Ohzuku, H. Tamura, K. Sawai, J. Electrochem. Soc. 144 (1997).
[28] Y. Itou, Y. Ukyo, J. Power Sources 146 (2005) 39.
[29] E. Markervich, G. Salitra, M. Levi, D. Aurbach, J. Power Sources 146 (2005) 146.
[30] H. Gabrisch, J. Wilcox, M. Doeff, Electrochem. Solid-State Lett. 11 (2008) A25.
[31] G. Singh, G. Ceder, M. Bazant, Electrochim. Acta 53 (2008) 7599.
[32] C. Delmas, M. Maccario, L. Croguennec, F.L. Cras, F. Weill, Nat. Mater. 7 (2008) 665.
[33] C. Wang, A.M. Sastry, J. Electrochem. Soc. 154 (2007) A1035.
[34] D. Wang, X. Wu, Z. Wang, L. Chen, J. Power Sources 140 (2005) 125.
[35] S. Komaba, N. Kumagai, Y. Kataoka, Electrochim. Acta 47 (2002) 1229.